Inorganic Chemistry

Article

pubs.acs.org/IC

Insights into the Mechanisms of Amyloid Formation of Zn^{II}-Ab11-28: pH-Dependent Zinc Coordination and Overall Charge as Key Parameters for Kinetics and the Structure of Zn^{II}-Ab11-28 Aggregates

Bruno Alies,[†,‡] Giovanni LaPenna,[§] Stéphanie Sayen,[⊥] Emmanuel Guillon,[⊥] Christelle Hureau,*[,†,‡] and Peter Faller*[,†,‡]

[†]LCC (Laboratoire de Chimie de Coordination), CNRS, 205 route de Narbonne, BP 44099, F-31077 Toulouse Cedex 4, France

[‡]Université de Toulouse, UPS, INPT, F-31077 Toulouse Cedex 4, France

[§]CNR-National Research Council of Italy, ICCOM, via Madonna del Piano 10, 50019 Sesto Fiorentino, Florence, Italy

[⊥]Institut de Chimie Moléculaire de Reims (ICMR, CNRS UMR 7312), Groupe de Chimie de Coordination, Université de Reims Champagne-Ardenne, BP 1039, 51687 Reims Cedex 2, France

Supporting Information

ABSTRACT: Self-assembly of amyloidogenic peptides and their metal complexes are of multiple interest including their association with several neurological diseases. Therefore, a better understanding of the role of metal ions in the aggregation process is of broad interest. We report pH-dependent structural and aggregation studies on Zn^{II} binding to the amyloidogenic peptide Ab11-28. The results suggest that coordination of the N-terminal amine to Zn^{II} is responsible for the inhibition of amyloid formation and the overall charge for amorphous aggregates.

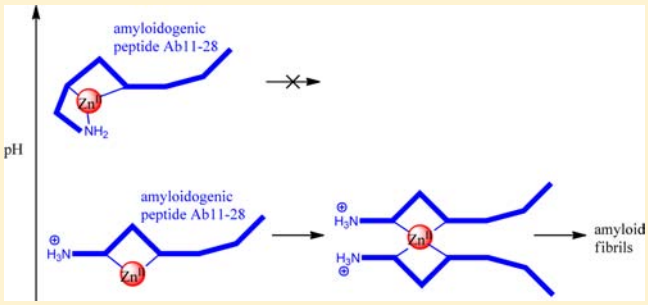

INTRODUCTION

The supramolecular assembly of peptides and proteins into amyloid fibrils is intensively studied owing to their important biological roles including different neurological diseases (Alzheimer's, Parkinson's, etc.)[1−3] and because amyloids are of interest in material science.[4,5] Amyloids are made of peptides or proteins that adopt fibrils based on the cross-β-structure, in which the peptide backbone is orthogonal to the fibril axis.[4,6,7] They are normally formed by a two-step process of slow nucleation, followed by a typically fast, autocatalytic surface growth, leading to a sigmoid curve for amyloid formation.[8]

The binding of metal ions such as zinc, copper, and iron to amyloidogenic peptides modulates the aggregation behavior[9−14] and results in fibrils with embedded metal ions.[15−20] The use of small peptides to model the aggregation of native peptides or to gain general insight into the mechanisms was very helpful in the understanding of amyloid formation[4,21−23] and the role of metal ions.[24−30] Smaller model peptides are often easier to handle and have higher reproducibility in terms of aggregation behavior.

In the past, we investigated the effect of Zn^{II} and Cu^{II} binding on three different amyloidogenic model peptides and found metal- and peptide-specific effects related to the coordination chemistry of the metal ions.[31,32] One of these peptides, Ab11-28, showed suitable properties in terms of mechanistic studies for Zn^{II}-induced aggregation. Ab11-28 is derived from amyloid-β (Aβ) peptide, which plays a crucial role in Alzheimer's disease. Although Ab11-28 is missing the N- and C-terminal parts and, hence, is clearly different from Aβ in terms of aggregation and metal binding,[33] it preserves two important features for metal-induced amyloid formation. These are the two His residues (His13 and His14) known to anchor Zn^{II} and the hydrophobic core (amino acid residues spanning from 17 to 21, sequence LVFFA). Moreover, truncated Aβ peptides starting at position 11 (i.e., Aβ11-x) have been found in human amyloid plaques and are thus physiologically relevant.[34] Therefore, the amyloidogenic Ab11-28 peptide can serve as a model system to gain general insight into metal-induced amyloid formation.

Further studies on Zn^{II} binding to the peptide Ab11-28 at pH 7.4 showed the importance of dynamical Zn^{II} binding for aggregation and suggested that the formation of a transitory complex of two Ab11-28 bound to Zn^{II} (i.e., $Zn^{II}(Ab11\text{-}28)_2$) via His14 and the carboxylate of Glu11 is most prone to fibril formation.[35]

In order to gain insight into the relationships between the structure of Zn^{II} binding and the aggregation behavior, we studied the pH dependence of Zn^{II} binding to Ab11-28 upon aggregation.

Received: May 10, 2012
Published: July 5, 2012

dx.doi.org/10.1021/ic300972j | Inorg. Chem. 2012, 51, 7897−7902

RESULTS AND DISCUSSION

pH Dependence of $Zn^{II}_{0.5}$-Ab11-28 Aggregation. Our previous studies indicated that $Zn^{II}(Ab11\text{-}28)_2$ is the building block of aggregation into amyloids.[31,35] Changing the pH of metallopeptides like $Zn^{II}(Ab11\text{-}28)_2$ will influence two important parameters concerning aggregation: (i) the overall charge of a peptide is pH-dependent, and aggregation is classically faster when the overall charge approaches zero (Table 1).[36,37] (ii) Metal binding is often pH-dependent, and hence the structure of the metal−peptide complex can change.

Table 1. Expected Charge of Ab11-28 and $Zn^{II}_1(Ab11\text{-}28)_2$

pH	Ab11-28	Zn^{II}_1-$(Ab11\text{-}28)_2$
8.4	−2	−2
7.3	−1	0
6.3	0	+2

The aggregation of Ab11-28 with 0.5 equiv of Zn^{II} was followed by thioflavin T (ThT) fluorescence and turbidimetry at different pH values. ThT is a specific fluorescence dye for amyloid-type aggregates, while turbidity measures more amorphous aggregates because it depends mostly on the amount and size of aggregates.

Figure 1 (top) shows the time courses of the ThT fluorescence and turbidity of Ab11-28 with 0.5 equiv of Zn^{II} at pH 7. For either measurement, the overall curve has a sigmoidal form, and hence a $t_{1/2}$ and a plateau intensity can be estimated as indicated. $t_{1/2}$ of turbidity is shorter than $t_{1/2}$ from ThT, indicating that first amorphous-type aggregates are formed, which are subsequently transformed into amyloid-type aggregates.

The pH dependence of Ab11-28 with 0.5 equiv of Zn^{II} revealed very different ThT fluorescence and turbidity features (Figure 1, middle and bottom), indicating that aggregates and amyloid formation are not directly correlated. The main kinetic phase of ThT fluorescence was faster with lower pH (Figure 1, bottom), but the plateau reached at the end was similar (Figure 1, middle). This indicates that the same amount of amyloid was formed over the present pH range, but the formation was faster at low pH. In contrast, the turbidity increased rapidly in a nonsigmoidal manner and ThT fluorescence preceded (at the pH where it could be well measured, i.e., ≥ pH 7). The kinetics was not very sensitive to the pH (Figure 1, bottom). This suggests that amorphous, unstructured aggregates are formed before amyloids and likely a transformation occurred. The turbidity plateau reached was pH-dependent (Figure 1, middle). It was maximal around pH 7.4, i.e., increased from pH 8.4 to 7.4, and then decreased by a further lowering of the pH to 6.

To gain insight into the structural changes responsible for the pH dependence of turbidity and ThT fluorescence, NMR and X-ray absorption spectroscopies (XAS) were applied.

NMR. The effect of the addition of Zn^{II} to Ab11-28 was studied by ^{1}H NMR at several pH values (Figure 2). Measurements were done immediately after Zn^{II} addition in order to minimize aggregation. Zn^{II}-induced line broadening and shifts for some specific resonances (Figures 2 and S2 in the Supporting Information), indicating the specific binding of Zn^{II} to the affected residues. Figure 2, left panel, shows the aromatic region, including His13, His14, Phe19, and Phe20. Zn^{II} addition at different pH values lead to line broadening and to

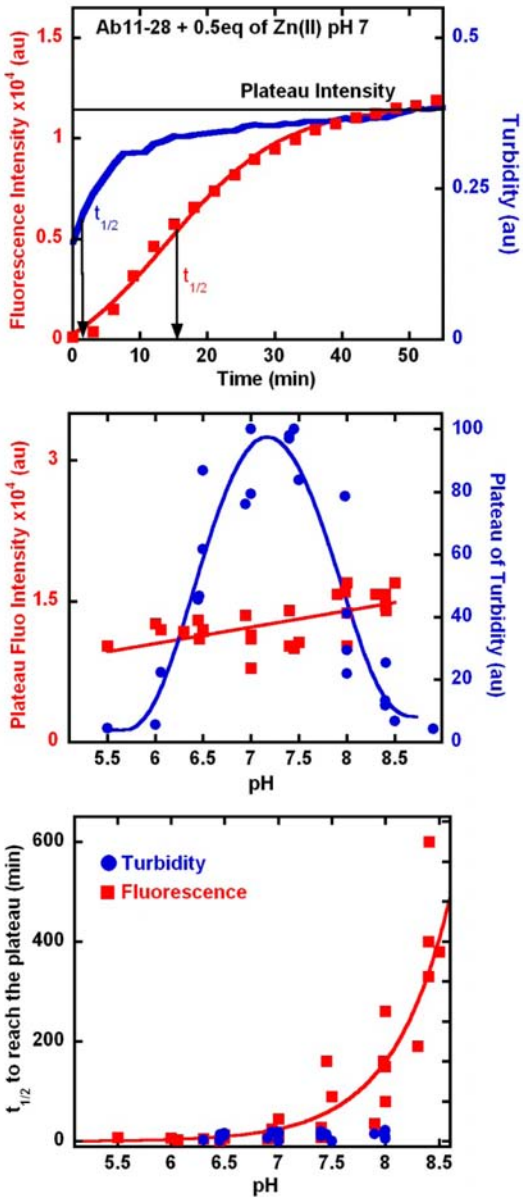

Figure 1. (Top) Time course of turbidity (blue, right scale) and ThT fluorescence (red squares, raw data; red line, fitted data; left scale) of Ab11-28 with 0.5 equiv of Zn^{II} at pH 7.0. The black line indicates the intensity of the plateau. $t_{1/2}$ values are given by the fit. (Middle) pH dependence of the plateau intensity reached in ThT fluorescence (red squares, raw data; red line, linear fit; left scale) and in turbidity (blue circles, raw data; blue line, trendline; right scale) by Ab11-28 with 0.5 equiv of Zn^{II} aggregation. Raw data are from five independent measurements. (Bottom) pH dependence of $t_{1/2}$ to reach the plateau in fluorescence (red square, raw data; red line, trendline) and in turbidity (blue circle) by Ab11-28 with 0.5 equiv of Zn^{II} aggregation. Raw data are from five independent measurements.

shifts of H−Cδ and H−Cε of His14. In contrast, the H−Cδ and H−Cε resonances of His13 were only little affected, showing a slight broadening and a slight chemical shift. The resonances of the two Phe are not affected at all, indicating no binding to or near the Phe. This indicates that over the pH range studied, His14, but not His13, is bound to Zn^{II}.

The resonance of H−Cα of Glu11 in the *apo*-Ab11-28 underwent a large shift over the pH range 7−9, in line with deprotonation of the N-terminal amine (Glu11). A pK_a of 7.8 is

dx.doi.org/10.1021/ic300972j | Inorg. Chem. 2012, 51, 7897−7902

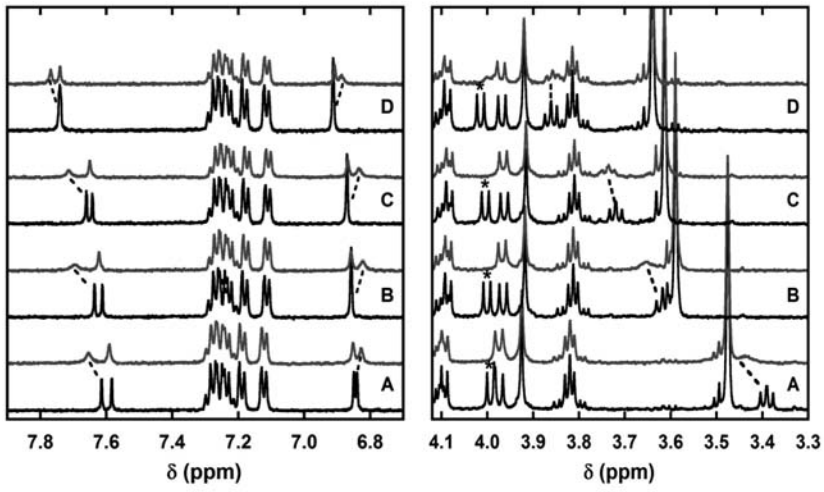

Figure 2. ^{1}H NMR of *apo*-Ab11-28 (lower trace) and Zn^{II}-Ab11-28 (upper trace) at pH 9.1 (A), 8.0 (B), 7.7 (C), and 7.3 (D) in the regions of H−Cδ and H−Cε of His13 and 14 (left) and H−Cα of Glu11 (right). Dotted lines represent the affected H−Cδ and H−Cε of His14 by Ab11-28 (left) and H−Cα of Glu11 (right). H−Cα of Glu11 shifts strongly because of protonation of NH_2. The asterisk indicates the H−Cα attributed to Val 12. Conditions: 300 μM Ab11-28, 270 μM Zn^{2+}, Tris-d_{11} 100 mM.

estimated, a typical value for N-terminal amines in peptides (Figure S3 in the Supporting Information). The addition of Zn^{II} showed a pH-dependent feature; at higher pH, the resonances shifted and were largely broadened; in contrast, at lower pH, no shift was induced and only a little broadening occurred (Figures 2 and S3 in the Supporting Information). This is interpreted in the sense that at higher pH the deprotonated NH_2 of the N-terminal Glu is a ligand to Zn^{II} but not at lower pH, where NH_3^+ is present. The smaller broadening at lower pH is ascribed to the binding of Zn^{II} to the COO^- of Glu11 (in line with ref 38).

These results suggest that Zn^{II} binding occurs to Glu11 and His14. In order to confirm this, we used the shorter, nonaggregating peptide Ab11-14 (Glu-Val-His-His-NH_2), and as expected, the same resonances were affected by the addition of Zn^{II} in a way very similar to that in the longer Ab11-28 (see above). Moreover, the same pH dependence was observed (see Figure S4 in the Supporting Information) and hence supports the binding of Zn^{II} by NH_2 of Glu11 at higher pH.

XAS. X-ray absorption near-edge structure (XANES) spectra give an indication of the dominant zinc species in a given sample. Thus, XANES was used to probe the pH dependence of Zn^{II} coordination to Ab11-28 (Figure 3). The Zn K-edge spectra for the two Ab11-28 with 0.5 equiv of Zn^{II} at pH 6.5 and 7.5 were similar, indicating that no major difference in zinc speciation occurred between these two pH values. On the contrary, the sample at pH 8.5 exhibited a different shape. Indeed, based qualitatively on the shapes of the main white-line peak at ~9665 eV and oscillations on the high energy side of the white-line peak, the solution at pH 8.5 had distinctly a different spectrum compared with those at lower pH. The white-line peak was enlarged with pH, especially between pH 7.5 and 8.5, the peak at 9670 eV was shifted to a higher energy (~9672 eV), and the peak at 9678 eV (dotted line) disappeared. These differences indicate a change in coordination between pH 7.5 and 8.5 in line with the NMR data (see above).

Previous studies suggested that the dimer $Zn^{II}(Ab11\text{-}28)_2$ is the building block, which first forms nonamyloid aggregates (the presence of turbidity but no ThT fluorescence) and then

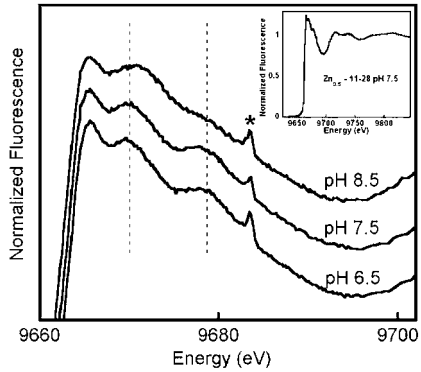

Figure 3. Zoom on XANES of Ab11-28 with 0.5 equiv of Zn^{II} at pH 6.5, 7.5, and 8.5. The asterisk indicates an artifact of the detector (inset: complete XANES of Ab11-28 with 0.5 equiv of Zn^{II} at pH 7.5).

converts to amyloid fibril (increasing ThT fluorescence). Moreover, Zn^{II} was bound by COO^- from two Glu11 and two imidazole of His14 from each peptide[38,39] (see the inset in Figure 4A). As pointed out by a reviewer, the binding of Zn^{II} to Glu11 and His14 is not consistent with a β-sheet structure of this portion of the peptide because the two side chains point in opposite directions. This resembles the structure from solid-state NMR of Aβ1-42, in which the N-terminal part 1−16 is disordered and the β-sheet structure starts around position 17.[40,41] The structural data obtained above suggest that the Zn^{II} binding in $Zn^{II}(Ab11\text{-}28)_2$ is pH-dependent in the region of pH 6−8.5. Two forms exist with an apparent pK_a of about 7.8, the low pH form binds His14 and COO^- of Glu11, and in the high pH form, the N-terminal amine binds additionally to His14. Whether COO^- is still bound cannot be determined.

The pK_a of N-terminal amine binding to Zn^{II} correlates very well with the kinetics of the fibril formation measured by ThT (Figure 1, bottom) and hence suggests that the binding of the N-terminal amine changes the peptide structure to a less aggregation-prone conformation. An explanation would be that additional binding of N-terminal NH_2 to Zn^{II} coordinated by COO^- from Glu11 and His14 of the two peptides might inhibit the alignment of the two portions from amino acids 15−28 in a

dx.doi.org/10.1021/ic300972j | Inorg. Chem. 2012, 51, 7897−7902

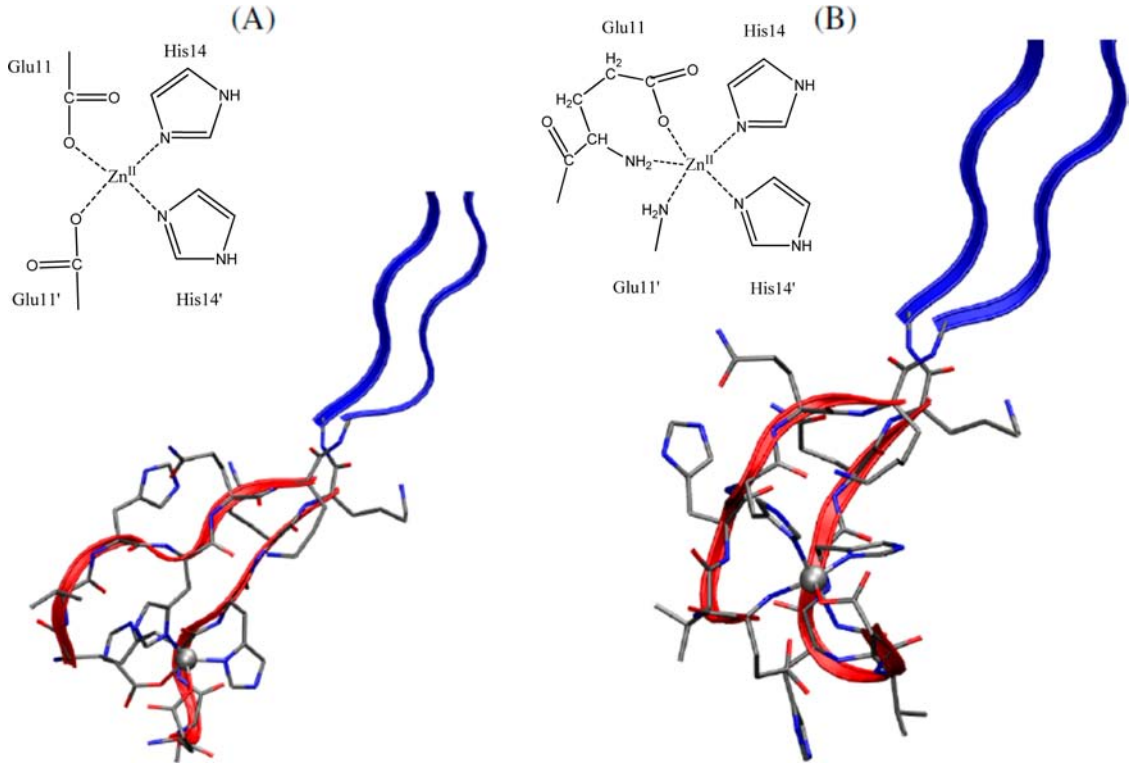

Figure 4. Final configurations (t = 5 ps) for models 1 (low pH, panel A) and 2 (high pH, panel B) for TB-MD at T = 50 K. Residues 17−28 (displayed as ribbons only) are represented with the positions of the empirical models. Residues 11−16 are represented as sticks, and Zn^{II} is represented as a sphere. Bonds involving Zn^{II} are displayed for interatomic distances within 2.2 Å. Atomic radii are arbitrary, and the color scheme is gray for C, red for O, blue for N, and silver for Cu. The *VMD* program was used for this and the following molecular drawings. A schematic view of the first coordination sphere for the two structures is given in the upper left corner.

parallel β-sheet as needed for an amyloid structure. It might also reduce dimerization because the monomeric $Zn^{II}{}_1(Ab11\text{-}28)_1$ is stabilized because of the tripodal binding of NH_2, COO^- from Glu11, and His14.

Modeling. To gain deeper insight into the possible structural changes of the Zn^{II} site at different pH values and of the implications of structural changes on the peptide structure and aggregation, we investigated two semiempirical models of the dimeric $Zn^{II}(Ab11-28)_2$ with NH_3^+-Ab11-28 and NH_2-Ab11-28, respectively, as ligands.

First, $Zn^{II}(Ab11\text{-}28)_2$ with two NH_3^+-Ab11-28, in which zinc is bound to both His14 residues via the Nδ atoms, as suggested by ref 38, and to both COO^- groups of Glu11, was constructed and simulated in the vacuum at T = 50 K for 5 ps. This corresponds to $Zn^{II}(Ab11\text{-}28)_2$ at pH 6.5, called model 1 hereafter. Then, a second model, $Zn^{II}(Ab11\text{-}28)_2$ with two NH_2-Ab11-28, in which the two N atoms of the two Glu11 residues are included in the zinc coordination sphere corresponding to $Zn^{II}(Ab11\text{-}28)_2$ at pH 8.5 was simulated in the same conditions (model 2 hereafter).

The result of model 1 is very similar to the structure reported by Kozin and co-workers (Figure 4a in ref 38), although in their peptide, the NH_2 of Glu11 is acetylated. Thus, a significant difference in our model 1 is that the N termini are positively charged and one is in hydrogen-bond distance to COO^- (Figure 4a).

Once the N termini are deprotonated and the approach of N(Glu 11) toward Zn^{II} is forced (model 2), one of the COO^- groups of Glu11 is expelled away from the zinc coordination sphere. This event produces a pentacoordinated Zn^{II} (ligands 2 His, 2 NH_2, and 1 COO^-; Figure 4B), which is stable for the simulated time.

The root-mean-square deviation (rmsd) of backbone heavy atoms in the two models measured for residues 11−16 with respect to the initial extended β-sheet conformation (almost the backbone structure proposed by Luhrs et al.[40]) is smaller for model 1 (low pH) than for model 2 (high pH) (the two 5-ps-range curves in Figure 5). This indicates a distortion of the β-sheet alignment between the two peptides in the high-pH

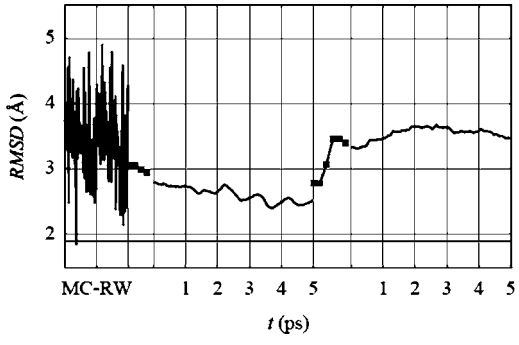

Figure 5. rmsd for heavy backbone atoms along with different trajectories. The first noisy line represents the span of values obtained within the MC-RW of residues 11−13. Square points represent the values along with the manipulations of empirical models (see the text for details). The two lines along with the 5-ps trajectories are the values for the TB-MD at T = 50 K. The first 5-ps part is for model 1, and the second 5-ps part is for model 2.

dx.doi.org/10.1021/ic300972j | *Inorg. Chem.* 2012, 51, 7897−7902

model, induced by the NH_2(Glu 11)−Zn^{II} bond. This observation is in line with a lower propensity to aggregate.

It is interesting to note that the turbidity does not correlate with the changes of Zn^{II} coordination observed because the intensity was highest around pH 7.4 (Figure 1, middle) and the kinetics is much less pH-dependent than it is for ThT (Figure 1, bottom). This can be explained by the overall net charge, which is an important parameter of aggregation because classically proteins precipitate better the closer the pH is to the isoelectric point (pI). The overall expected charges of $Zn^{II}{}_1$(Ab11-28)$_2$ is around 0 at pH 7.4 (Table 1) and thus very well with the profile of turbidity measurements (see Figure 1, middle), where a bell-like curve in aggregation/precipitation dependent on the pH was found with a peak around pH 7.4.

In conclusion, the very different pH dependences of ThT fluorescence (related to amyloids) and turbidity (global aggregation state) can be explained. The precipitation of $Zn^{II}{}_1$(Ab11-28)$_2$ leading to high turbidity is governed by the global charge of $Zn^{II}{}_1$(Ab11−28)$_2$, whereas the amyloid formation is governed by the pH-dependent structure of the zinc(II) peptide complex.

MATERIALS AND METHODS

Ab11-28 Sample Preparation. The peptide Ab11-28 (sequence Glu-Val-His-His-Gln-Lys-Leu-Val-Phe-Phe-Ala-Glu-Asp-Val-Gly-Ser-Asn-Lys) was purchased from GenScript Corp. (Piscataway, NJ). The stock solutions of Ab11-28 (∼1.2 mM) have been prepared by dissolving the peptide in Milli-Q water (resistivity = 18 MΩ cm^{-1}) or in D_2O for an NMR stock solution, which resulted in a final pH of 2. The pH of the solution was then adjusted to pH 12 by the addition of NaOH (or NaOD for NMR) stock solutions, in order to monomerize the peptides. These stock solutions were stored at 253 K. The peptide concentrations were determined by using the molar extinction coefficient ε = 390 M^{-1} cm^{-1} of the two phenylalanines at 258 nm.[30] Because phenylalanine does not absorb at 275 nm, the absorption at that wavelength was subtracted in order to remove contributions from the buffer or baseline drifts. A Zn^{II} stock solution was prepared with $Zn^{II}SO_4$ monohydrate (Strem Chemicals) in water or in D_2O for NMR experiments. Aggregation of peptides in the presence of Zn^{II} has been performed by dissolving peptides from a stock solution into a 100 mM 4-(2-hydroxyethyl)-1-piperazineethanesulfonic acid buffer at pH 7.4, 100 mM piperazine-*N*,*N*′-bis(2-ethanesulfonic acid) for pH 7.0 and 6.5, 2-(*N*-morpholino)-ethanesulfonic acid for pH 6.0, or piperazine-1,4-bis(2-hydroxypropanesulfonic acid) for pH 8.0 and 8.4 and was controlled at the end of the experiment. All of the experiments measuring either turbidity or fluorescence intensity have been performed at 298 K. The experiments were repeated at least five times in different preparations.

UV−Vis Spectroscopy. UV−vis spectra were recorded on an Agilent 8453 UV−visible spectrometer. Measurements were performed at room temperature.

Turbimetry. Turbidity measurements were done by measuring the absorbance at 350 nm with a FLUOstar Optima (BMG Labtech) in a quartz microplate (96-well, Hellma). The final concentrations of Ab11-28 and ThT are 300 and 10 μM, respectively.

Fluorescence Spectroscopy. Fluorescence spectra were measured by using a FLUOstar Optima (BMG Labtech). ThT, Ab11-28, and Zn^{II} were mixed in a 100 mM buffer and placed in a 96-well microplate. The time course of ThT fluorescence was then measured (excitation, 440 nm; emission, 490 nm; bandwidth for emission and excitation, 10 nm). The final concentrations of Ab11-28 and ThT were 300 and 10 μM, respectively.

The sigmoidal ThT curve was fitted with the program *KaleidaGraph* to the formula $F(t) = F_0 + A/\{1 + \exp[-k(t - t^{1/2})]\}$, where k is the elongation rate, A the amplitude, $t_{1/2}$ the time point when half the maximal intensity is reached, and F_0 the baseline before aggregation.[42]

XAS. XANES measurements were carried out at the SOLEIL Synchrotron Facility (St. Aubin, France), which was operating with a ring current of 400 mA. Zn^{II} K-edge XAS spectra were collected on the SAMBA beamline. The measurements were performed using a Si(220) water-cooled double-crystal monochromator and two large silicon mirrors for high-energy harmonics rejection. Energy calibration was achieved by measuring a copper foil and assigning the first inflection point of the absorption spectrum to 8979 eV. The spectra were measured in fluorescence mode by measuring the Zn^{II} Kα fluorescence with a 7-element germanium detector. The liquid samples were injected in special sample holders and cooled down to 20−30 K using a helium-flow cryostat. XANES spectra were background-corrected by a linear regression through the preedge region and a polynomial through the postedge region and normalized to the edge jump.

NMR. NMR experiments were realized on a Avance 500 Bruker NMR spectrometer. Several solutions of the buffer deuterated tris(hydroxymethyl)aminomethane (D_{11}-TRIS) at different pH values were prepared by solubilization of the TRIS powder in D_2O and acidification with D_2SO_4. Ab11-28 samples were freshly prepared from a D_2O stock solution (see the Ab11-28 Sample Preparation section). Ab11-28 (final TRIS concentration of 300 μM) was added to several TRIS solutions at a given pH (final concentration of 100 mM). The solutions were mixed, the pH was measured (to take into account the increase of the pH due to the Ab11-28 solution), and the resulting solution was added to the NMR tube. The residual water signal was suppressed by a presaturation procedure. Zn^{II} was directly added to the NMR tube, and measurements were performed as quickly as possible (less than 1 min 30 s) in order to minimize the aggregation process during spectrum acquisition. The assignment of the resonances at pH 7.4 was published earlier,[35] and titration between pH 7 and 9 in small pH steps allowed the assignment of the resonances over this pH range (see Figure S4 in the Supporting Information).

Calculations. The first two monomers in the structure reported in ref 40 (PDB id2BEG) were used as templates for building the initial Ab11-28 dimer. The φ and ψ dihedral angles of each residue are, in this structure, approaching the pair of values φ = −120°/ψ = 120° typical of a parallel β-sheet. A Zn^{II} ion was docked within the Nd atoms of His14, by using a dummy counterion model,[43] and the two His14 side chains were adapted to bind the Zn^{II} ion in an approximate tetrahedral coordination. A short molecular dynamics (MD) trajectory (20 ps) of this model in the vacuum and at T = 50 K was performed, keeping the N, CA, and C atoms of residues 17−28 fixed in space, in order to adapt the Zn^{II}-bound 11−16 region to the extended β-strand proposed by Luhrs et al.[40]

All of the manipulations of the empirical models were performed with the *NAMD*[44] and *VMD*[45] packages, with external forces implemented via the *PLUMED*[46] plugins. In order to build structures with the two Glu11 side chains in the Zn^{II} coordination sphere already occupied by the two His14 side chains, a Monte Carlo random walk (MC-RW) for the dihedral angles involving heavy atoms in the two 11−13 regions was performed. This random walk[47] samples almost every configuration with nonoverlapping atoms, with residues 14−28 fixed in space. Among the collected configurations, the first configuration with one Zn^{II}Oe(Glu 11) distance (in both Glu11 residues) within 3 Å was extracted. This configuration was then moved into the closest energy minimum and assumed as the starting model for a semiempirical calculation based on the tight-binding (TB) approximation.[48] The system was truncated to the Zn^{II} complex of Ab(11−16)−CO−NH−CH_3. The density functional TB code DFTB +[49] was used with the set of parameters developed for organic Zn^{II} compounds.[50] After 300 steps of energy minimization, a 5-ps-long MD simulation at T = 50 K was performed with the C, O, and N atoms in the two −CO−NH−CH_3 C-terminal groups (mimicking the Lys16−Leu17 linkage) fixed in space. A time step of 1 fs was used with no thermal bath (approximately constant energy or Born−Oppenheimer MD simulation). The result is model 1.

The approach of the two N termini of Glu11 toward Zn^{II} (model 2) was performed by the removal of one proton for each N terminus in the last DFTB configuration. External harmonic forces acting on the

dx.doi.org/10.1021/ic300972j | Inorg. Chem. 2012, 51, 7897−7902

Zn^{II}–N(Glu 11) distances were added to the empirical model. By increasing the equilibrium distance for the harmonic force in steps of 0.5 Å, the N(Glu 11)–Zn(II) distance decreased from 4.5 to 2 Å, ending to a model where both N(Glu 11) atoms are at bonding distance with Zn^{II}. The final configuration obtained with this procedure was used as the starting point for a second DFTB simulation, again at T = 50 K for 5 ps. The result is model 2.

■ ASSOCIATED CONTENT

Ⓢ Supporting Information

ThT fluorescence and turbidity, ^{1}H NMR spectra, and chemical shift of H–Cα of the N-terminal atom. This material is available free of charge via the Internet at http://pubs.acs.org.

■ AUTHOR INFORMATION

Corresponding Author

*E-mail: christelle.hureau@lcc-toulouse.fr (C.H.), peter.faller@lcc-toulouse.fr (P.F.). Tel: +33 5 61 33 31 62.

Notes

The authors declare no competing financial interest.

■ ACKNOWLEDGMENTS

Financial support from the "Region Midi-Pyrénées" (Research Grant APRTCN09004783) is acknowledged. We acknowledge SOLEIL for provision of synchrotron radiation on the SAMBA beamline (Proposal 20100771) and Stéphanie Belin (SOLEIL) and Christian Bijani for XAS and NMR measurements, respectively.

■ REFERENCES

(1) Haass, C.; Selkoe, D. J. *Nat. Rev. Mol. Cell Biol.* **2007**, *8*, 101–112.
(2) Chiti, F.; Dobson, C. M. *Annu. Rev. Biochem.* **2006**, *75*, 333–366.
(3) Fowler, D. M.; Koulov, A. V.; Balch, W. E.; Kelly, J. W. *Trends Biochem. Sci.* **2007**, *32* (5), 217–224.
(4) Hamley, I. W. *Angew. Chem., Int. Ed.* **2007**, *46* (43), 8128–8147.
(5) Gazit, E. *Chem. Soc. Rev.* **2007**, *36* (8), 1263–1269.
(6) Cherny, I.; Gazit, E. *Angew. Chem., Int. Ed.* **2008**, *47* (22), 4062–4069.
(7) Morris, K.; Serpell, L. *Chem. Soc. Rev.* **2010**, *39* (9), 3445–3453.
(8) Morris, A. M.; Watzky, M. A.; Agar, J. N.; Finke, R. G. *Biochemistry* **2008**, *47* (8), 2413–2427.
(9) Exley, C. *J. Alzheimer's Dis* **2006**, *10* (2–3), 173–177.
(10) Barnham, K. J.; Cappai, R.; Beyreuther, K.; Masters, C. L.; Hill, A. F. *Trends Biochem. Sci.* **2006**, *31* (8), 465–472.
(11) Tougu, V.; Tiiman, A.; Palumaa, P. *Metallomics* **2011**, *3* (3), 250–261.
(12) Hong, L.; Simon, J. D. *Metallomics* **2011**, *3* (3), 262–266.
(13) Perez, L. R.; Franz, K. J., *Dalton Trans. 39* (9), 2177–2187.
(14) Calabrese, M. F.; Miranker, A. D. *Prion* **2009**, *3* (1), 1–4.
(15) Brown, D. R. *Dalton Trans.* **2009**, *21*, 4069–4076.
(16) Faller, P.; Hureau, C. *Dalton Trans.* **2009**, 1080–1094.
(17) Drago, D.; Bolognin, S.; Zatta, P. *Curr. Alzheimer Res.* **2008**, *5* (6), 500–507.
(18) Fritz, G.; Botelho, H. M.; Morozova-Roche, L. A.; Gomes, C. M. *FEBS J* **2010**, *277* (22), 4578–4590.
(19) Duce, J. A.; Bush, A. I. *Prog. Neurobiol. 92* (1), 1–18.
(20) Gaggelli, E.; Kozlowski, H.; Valensin, D.; Valensin, G. *Chem. Rev.* **2006**, *106* (6), 1995–2044.
(21) Gazit, E. *Prion* **2007**, *1* (1), 32–35.
(22) Lynn, D. G.; Meredith, S. C. *J. Struct. Biol.* **2000**, *130* (2–3), 153–173.
(23) Eisenberg, D.; Nelson, R.; Sawaya, M. R.; Balbirnie, M.; Sambashivan, S.; Ivanova, M. I.; Madsen, A. O.; Riekel, C. *Acc. Chem. Res.* **2006**, *39* (9), 568–575.
(24) Yang, H.; Pritzker, M.; Fung, S. Y.; Sheng, Y.; Wang, W.; Chen, P. *Langmuir* **2006**, *22* (20), 8553–8562.
(25) Pagel, K.; Seri, T.; von Berlepsch, H.; Griebel, J.; Kirmse, R.; Bottcher, C.; Koksch, B. *ChemBioChem* **2008**, *9* (4), 531–536.
(26) Hoernke, M.; Koksch, B.; Brezesinski, G. *Biophys. Chem.* **2010**, *150* (1–3), 64–72.
(27) Schlosser, G.; Stefanescu, R.; Przybylski, M.; Murariu, M.; Hudecz, F.; Drochioiu, G. *Eur. J. Mass Spectrom. (Chichester, England)* **2007**, *13* (5), 331–337.
(28) Dong, J.; Canfield, J. M.; Mehta, A. K.; Shokes, J. E.; Tian, B.; Childers, W. S.; Simmons, J. A.; Mao, Z.; Scott, R. A.; Warncke, K.; Lynn, D. G. *Proc. Natl. Acad. Sci. U.S.A.* **2007**, *104* (33), 13313–13318.
(29) Dong, J.; Shokes, J. E.; Scott, R. A.; Lynn, D. G. *J. Am. Chem. Soc.* **2006**, *128* (11), 3540–3542.
(30) Scotter, A. J.; Guo, M.; Tomczak, M. M.; Daley, M. E.; Campbell, R. L.; Oko, R. J.; Bateman, D. A.; Chakrabartty, A.; Sykes, B. D.; Davies, P. L. *BMC Struct. Biol.* **2007**, *7*, 63.
(31) Alies, B.; Pradines, V.; Llorens-Alliot, I.; Sayen, S.; Guillon, E.; Hureau, C.; Faller, P. *J. Biol. Inorg. Chem.* **2011**, *16* (2), 333–340.
(32) Pradines, V.; Jurca Stoia, A.; Faller, P. *New J. Chem.* **2009**, *32*, 1189–1194.
(33) Tougu, V.; Palumaa, P. *Coord. Chem. Rev.* **2012**, DOI: 10.1016/j.ccr.2011.12.008.
(34) Tekirian, T. L. *J. Alzheimer's Dis.* **2001**, *3* (2), 241–248.
(35) Alies, B.; Solari, P. L.; Hureau, C.; Faller, P. *Inorg. Chem.* **2012**, *51* (1), 701–708.
(36) Chiti, F.; Stefani, M.; Taddei, N.; Ramponi, G.; Dobson, C. M. *Nature* **2003**, *424* (6950), 805–808.
(37) Lopez De La Paz, M.; Goldie, K.; Zurdo, J.; Lacroix, E.; Dobson, C. M.; Hoenger, A.; Serrano, L. *Proc. Natl. Acad. Sci. U.S.A.* **2002**, *99* (25), 16052–7.
(38) Tsvetkov, P. O.; Kulikova, A. A.; Golovin, A. V.; Tkachev, Y. V.; Archakov, A. I.; Kozin, S. A.; Makarov, A. A. *Biophys. J.* **2010**, *99* (10), L84–L86.
(39) Kozin, S. A.; Mezentsev, Y. V.; Kulikova, A. A.; Indeykina, M. I.; Golovin, A. V.; Ivanov, A. S.; Tsvetkov, P. O.; Makarov, A. A. *Mol. Biosyst.* **2011**, *7* (4), 1053–1055.
(40) Luhrs, T.; Ritter, C.; Adrian, M.; Riek-Loher, D.; Bohrmann, B.; Dobeli, H.; Schubert, D.; Riek, R. *Proc. Natl. Acad. Sci. U.S.A.* **2005**, *102* (48), 17342–17347.
(41) Tycko, R. *Q. Rev. Biophys.* **2006**, *39* (1), 1–55.
(42) Hellstrand, E.; Boland, B.; Walsh, D. M.; Linse, S. *ACS Chem. Neurosci.* **2009**, *1*, 13–18.
(43) Pang, Y. P.; Xu, K.; Yazal, J. E.; Prendergas, F. G. *Protein Sci.* **2000**, *9* (10), 1857–1865.
(44) Phillips, J. C.; Braun, R.; Wang, W.; Gumbart, J.; Tajkhorshid, E.; Villa, E.; Chipot, C.; Skeel, R. D.; Kale, L.; Schulten, K. *J. Comput. Chem.* **2005**, *26* (16), 1781–1802.
(45) Humphrey, W.; Dalke, A.; Schulten, K. *J. Mol. Graph.* **1996**, *14* (1), 33–38, 27–28.
(46) Bonomi, M.; Branduardi, D.; Bussi, G.; Camilloni, C.; Provasi, D.; Raiteri, P.; Donadio, D.; Marinelli, F.; Pietrucci, F.; Broglia, R. A.; Parrinello, M. *Comput. Phys. Commun.* **2009**, *180* (10), 1961–1972.
(47) La Penna, G.; Morante, S.; Perico, A.; Rossi, G. C. *J. Chem. Phys.* **2004**, *121* (21), 10725–10741.
(48) Colombo, L. *Riv. Nuovo Cimento Soc. Ital. Fis.* **2005**, *28* (10), 1–59.
(49) Aradi, B.; Hourahine, B.; Frauenheim, T. *J. Phys. Chem. A* **2007**, *111* (26), 5678–5684.
(50) Moreira, N. H.; Dolgonos, G.; Aradi, B.; da Rosa, A. L.; Frauenheim, T. *J. Chem. Theory Comput.* **2009**, *5* (3), 605–614.